

LONG-DISTANCE MicroPIV MEASUREMENTS OF A COMMERCIAL AIRCRAFT MODEL AT LOW REYNOLDS NUMBER

F. Gökhan Ergin¹
Dantec Dynamics
Skovlunde, Denmark

Nafiz Alemdaroğlu²
METU
Ankara, Turkey

ABSTRACT

Velocity measurements from a sufficiently long standoff distance with micron scale resolution have significant potential in boundary layer flow diagnostics and in resolving small turbulent structures. Long-distance micro-Particle Image Velocimetry (LD μ PIV) technique is applied for velocity measurements around a commercial aircraft model. Experiments are performed using a closed-return open test section wind tunnel in combination with a single-camera LD μ PIV system. Two-dimensional, two-component (2D2C) velocity measurements are performed in a 12mm x 12mm field of view around the fuselage nose and in the wake of nose landing gear. The velocities are calculated using proven adaptive cross correlation algorithms. The instantaneous and averaged vector map results indicate that the LD μ PIV provides sufficient spatial resolution to perform nose stagnation flow, fuselage boundary layer and nose landing gear wake measurements.

INTRODUCTION

Boundary layer velocity measurements around streamlined bodies are often performed using point techniques like Constant Temperature Anemometry (CTA) or Laser Doppler Anemometry (LDA) due to their small measurement volumes and high spatial resolution. Although CTA provides a better frequency response and spatial resolution compared to LDA, it has a limitation in identifying the flow direction. LDA is preferred in situations where a flow reversal occurs, at the cost of reduced frequency response and/or spatial resolution. Regardless of the choice, both measurements provide velocity information in a point, and the identification of global modes and transient flow structures is not trivial, if at all possible.

Alternatively, Particle Image Velocimetry (PIV) can provide velocity information in a plane or in a volume, and finds many applications aerospace measurements; i.e. internal/external aerodynamics, separation bubbles, wakes, etc. Availability of long distance microscopes allows velocity measurements with micron-scale resolution from a distance, for example, in boundary layers. Since the technique is a variation of MicroPIV, it is conveniently named as Long Distance Micro PIV (LD μ PIV) [Adrian and Westerweel, 2010].

First application of LD μ PIV was used in the investigation of logarithmic layer in a turbulent pipe flow [Urushihara et al., 1993] where an in plane vector resolution of $\sim 250\mu\text{m}$ was achieved using a magnification of 6 on photographic film. Second application of this technique was the investigation of boundary layer flow disturbed by a small obstacle in a 1.0mmx1.3mm field of view (FOV) [Dieterle and Weichert, 1996] where the plane was illuminated from both directions to suppress potential particle motion due to radiation pressure. It was estimated that unidirectional laser radiation would accelerate stationary $1\mu\text{m}$ particles 0,5 m/s under the experimental conditions.

¹ Microfluidics Product Manager, Email: gokhan.ergin@dantecdynamics.com

² Prof. in Aerospace Engineering Department, Email: nafiz@metu.edu.tr

Lindken et al. [2002] used a reflecting type long-range microscope in a turbulent pipe flow experiment. The 380-nm-diameter silica fluorescent particles were imaged from a distance of 550 mm. A vector resolution of $42\mu\text{m}$ was achieved using 64×64 pixel interrogation area (IA), with number of spurious vectors less than 20% of the total number.

Kähler et al. [2005, 2006] applied LD μ PIV technique to measure the wall shear stress in a canonical boundary layer over a flat plate in order to verify the applicability of the “universal law-of-the-wall” suggested by Von Kármán. The authors systematically analysed the experimental limitations associated with seeding, illumination, out-of-focus particles, optical aberrations and correlation based vector calculations. The authors selected a refracting long-range microscope, compensated for image distortions and oriented the laser sheet illumination parallel to the surface to avoid unwanted reflections. Kähler et al. [2006] were successful in suppressing the unwanted wall reflections to an extent that they could image particle reflections from the flat surface. This information was used for the accurate estimation of the wall location. Kähler et al. [2005] concluded that systematic measurement error due to radiation pressure was small during the experiment, and can be neglected. Later, Kähler and Scholz [2006] applied the technique to investigate a laminar separation bubble on a 2D airfoil and a laminar round jet with 1mm orifice, the latter campaign using intensified high speed cameras.

Recently, Fisciatti et al. [2013] investigate a turbulent air jet flow using LD μ PIV and compare basic statistics with CTA measurements with good agreement between the results. They also use a reflecting type long-range microscope with 2.5x magnification at 580mm standoff distance, obtaining a vector resolution of $80\mu\text{m}$ with an IA of 64×64 pixels. By masking the spurious vectors at the edges of the image, they were able to achieve 94% reliable vectors in the measurement.

EXPERIMENTS

The experiments are performed in an open-test-section, closed-return compact wind tunnel with manual speed control up to 20 m/s (Figure 1a). The open test section dimensions are $120\times 120\times 205\text{ mm}^3$, and the 123-mm-long airplane model's frontal area covers only $\sim 3\%$ of the test section's cross sectional area. A smooth inlet fairing downstream of the test section ensures a smooth reentry of the air back in the wind tunnel. The metal airplane model is a 1:320-scale Boeing 737-800 manufactured by Shantou Wanchengfeng Craft Factory, and is mainly used as a gift to airline passengers. Additionally, the measurements are performed with the roll axis of the airplane aligned with the flow direction, far from the landing/take off trim of an actual aircraft. Therefore the results presented here do not aim to be indicative of the performance of the actual aircraft or actual flight conditions. Instead, the aim is to apply the LD μ PIV technique as a proof of concept in a small-scale experiment, where the experience can be applied to future work planned on boundary layer measurements. Since the metal airplane model is not transparent and had a shiny surface it was painted to black color to reduce reflections from the surface. The entire underbody of the fuselage was illuminated thru an opening using a DualPower 65-15 PIV laser head situated below the test section.

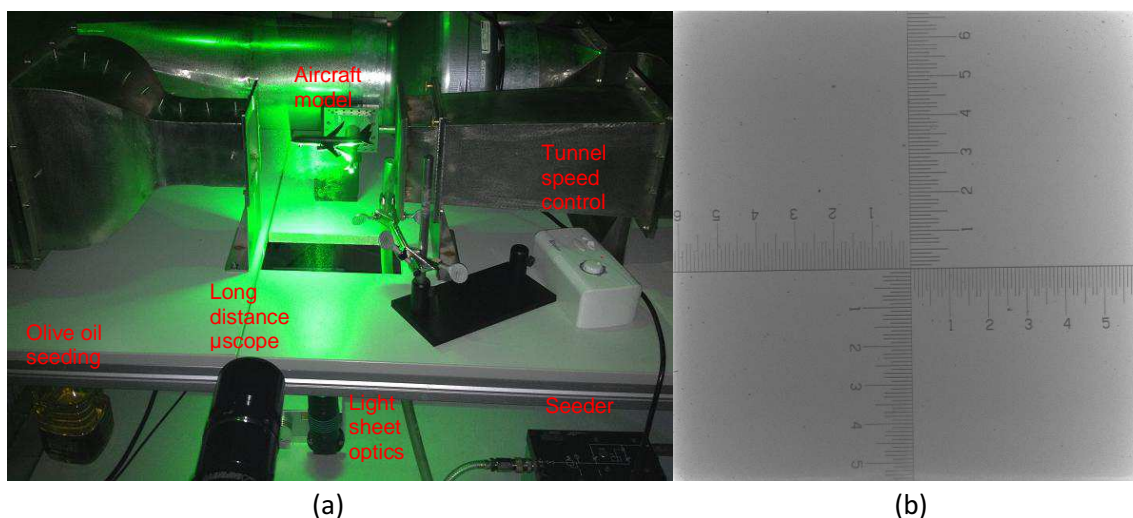


Figure 1: (a) Long-distance μ PIV experiment (b) Image of the cross ruler microPIV calibration target

The PIV laser system is a flashlamp-pumped, externally triggered, frequency-doubled, dual-cavity laser with Nd:YAG crystals emitting light at 532nm wavelength. Pulse energy on each cavity is separately adjustable using a motorized optical attenuator. Each cavity was operated at maximum pulse energy of 65mJ during the experiments. A vertical light sheet with 37-degree full angle was formed using a combination of commercial sheet formation optics; a 45-degree mirror, variable focus module and three cylindrical lenses. The light sheet was focused right below the fuselage surface, which is at a distance of 500mm, producing a thickness of 320 μ m, a confocal length of 20mm and an energy density of 60mJ/cm². The confocal length of the light sheet is larger than the 12.18x12.18mm² FOV, therefore the illuminated volume thickness can be assumed fairly constant in the entire FOV. The FOV is determined by performing a linear image calibration using a linear cross ruler target with 100 μ m resolution (Figure 1b).

Olive oil droplets are used as light scatterers. 1 μ m-mean-diameter droplets are generated using Dantec Dynamics 55L18 seeding generator and introduced in the wind tunnel downstream of the aircraft model for enhanced mixing and reduced flow disturbance (Figure 1a). Particle images are recorded in two regions, one in front of the fuselage nose ($U_o=11$ m/s) and one in the aft of the nose landing gear ($U_o=18$ m/s), from a nominal distance of 500mm using the refractive long-distance microscope at 1.25x total magnification. In this configuration the numerical aperture (NA) is 0.037 and the depth of field (DoF) is 390 μ m. Single-exposure image pairs are recorded with 12-bit depth using a FlowSense EO 4Mpix PIV camera, featuring a 55%-quantum efficiency CCD detector with 2048 square pixels in each direction. A typical raw particle image is included in Figure 3a. An interrogation window of 32x32 pix² sets the remaining dimensions of the measurement volume, i.e. 190x190x320 μ m³, and the 16 pix grid spacing corresponds to 95 μ m vector resolution.

The particle response time assuming Stokes flow is calculated as 2.8 μ s ($\tau_p = d_p^2 \rho_p / 18\mu$), which is on the same order of magnitude for the Kolmogorov time scale 2 μ s ($\tau_\eta = \eta / u_\eta$). This means that the seeding particles used in this experiment are not small enough to follow structures involved in turbulent dissipation ($\eta = 6\mu$ m), but are able to follow vortices that is limited by the vector resolution of the optical setup (~5x95 μ m).

The system synchronization is controlled with the system controller running DynamicStudio v3.41 software platform, which is also used for hardware control, database management, image processing and PIV analysis. Trigger signals are distributed thru an advanced synchronization unit with 12.5ns time resolution.

The adaptive cross-correlation (ACC) algorithm used in data processing is implemented in Dynamic Studio v3.41, the commercial PIV analysis package of Dantec Dynamics. Briefly, the implementation is an adaptive and iterative procedure: First, the displacement is calculated on an initial IA, which is larger in size compared to the final IA. Then the initial IA divided into smaller IA's, which are shifted by the displacement calculated in the previous step and deformed according to the velocity gradients in the image. Several passes can be made within each refinement step to further shift & deform the windows to minimize the in-plane particle dropout. The window deformation is performed by adapting the IA shape to velocity gradients. For each IA size, this procedure is repeated until a convergence limit in pixels or a maximum number of iterations is reached. Then a 9-point Gaussian fit is performed on the correlation peak to obtain the displacement field with subpixel accuracy in each pass. A number of FFT window (Hanning, Hamming etc.) and filter functions can be applied during the analysis. Finally, spurious vectors are identified and replaced with a number of validation schemes including peak height, peak height ratio, SNR & Universal Outlier Detection (UOD) [Westerweel and Scarano, 2005].

RESULTS

The vector results in Figure 2 are obtained averaging 61 vector maps at a nominal freestream velocity of 11m/s. Instantaneous vector maps are computed after an image background subtraction based on the minimum pixel value in the image ensemble. An ACC algorithm is used with a 50% overlapped, 32-pixel-wide square IA with no window refinement steps. A phase-only Gaussian filter is used in order to make the correlation more

tolerant to variations in the background. Spurious vectors are identified and replaced using a peak height ratio validation scheme (>1.2) in combination with a UOD [Westerweel and Scarano, 2005] in a 3×3 neighborhood with a detection threshold of 2.0 and a normalization level of 0.1 pixels. The convergence limit for deforming windows was 0.01 pixels or a maximum 10 iterations. No further FFT windowing or local smoothing is applied during the analysis. Every third vector is displayed in the horizontal plane and every second vector is displayed in the vertical plane. The number of spurious vectors was not more than 2% of the total number in the instantaneous vector maps. The average vector map is displayed with U and V components separately (Figure 2a, 2b) where stagnation flow at the nose tip is observed. An average boundary layer profile $U(y)$ along the blue line in Figure 2a is also displayed in Figure 2c without further smoothing. The vertical distance is measured in mm, but the origin is placed at an arbitrary location during image calibration. Since the profile is not obtained perpendicular to the surface, it cannot be compared to the Blasius profile. However, the flow in this region is quite laminar with no indication of turbulence in the instantaneous vector maps.

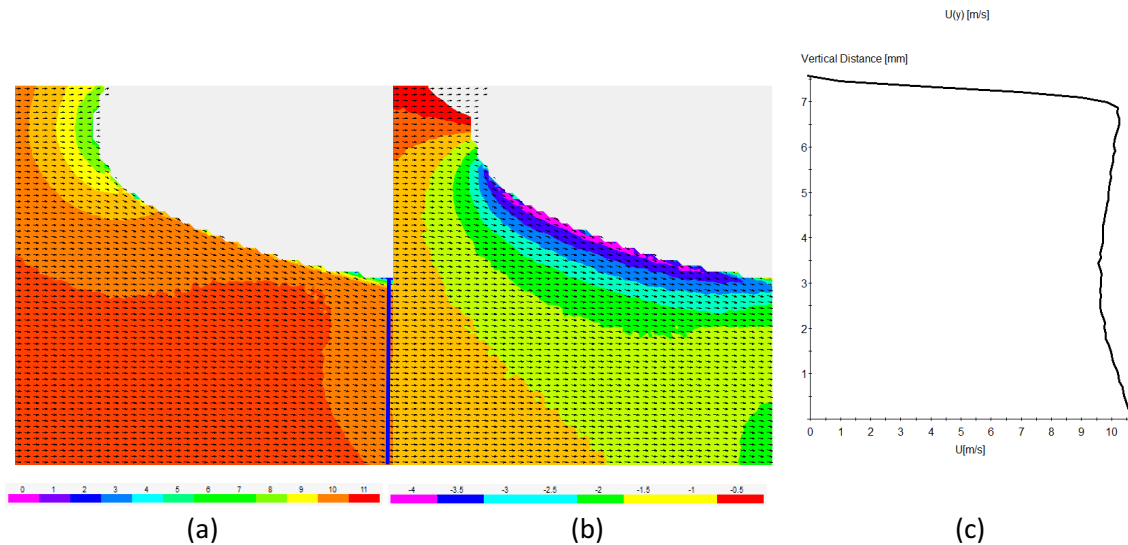


Figure 2: Average velocity results around the fuselage nose, with colors indicating (a) U component, (b) V component. (c) Boundary layer profile obtained along blue line in (a).

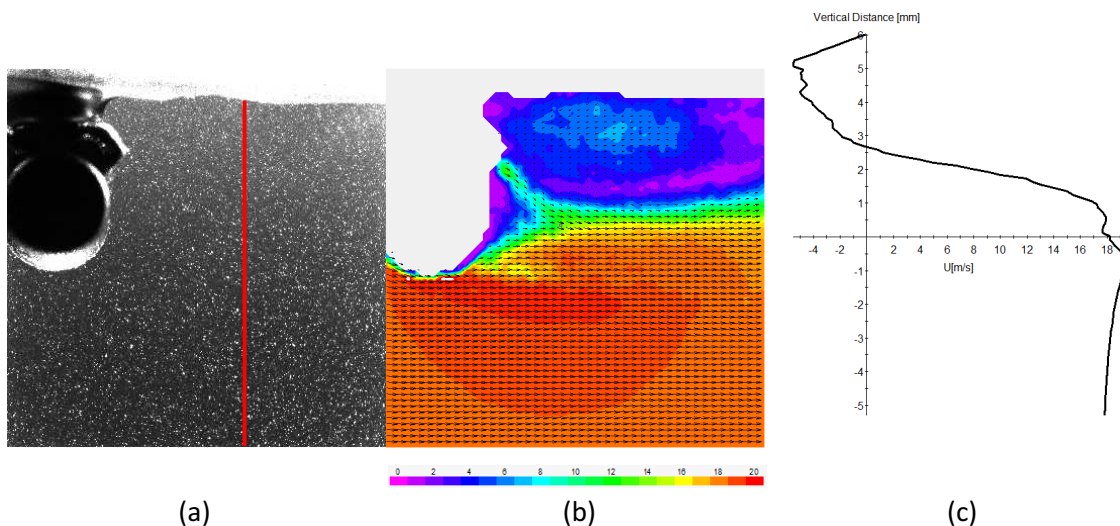


Figure 3: (a) Typical raw particle image, (b) average vector map with colors indicating vector length (c) velocity profile in the landing gear wake obtained along the red line in (a)

The vector results in Figure 3 are also obtained averaging 61 vector maps, but this time at a nominal freestream velocity of 18m/s. Instantaneous vector maps are computed in a similar fashion as explained above, except the IA size, which is chosen as 64×64 pixels. The number of spurious vectors was approximately 5% of the total number in the instantaneous vector maps. Once again the vector spacing is 16 pixels, so Figure 3b has the same vector density as in Figure 2a and 2b. The scalar field (colors) represents the vector length. One

immediate observation is the complex wake structure downstream of the wheel including a large rotational flow field. There is flow reversal close to the fuselage up to the landing gear strut, where the flow turns downwards and is entrained into the wake flow behind the wheel. The region with very small velocity is marked with purple color, which extends up to the right end of the FOV. A locally accelerated flow region is visible emerging from the lower part of the wheel. A boundary layer profile $U(y)$ along the red line in Figure 3a is also displayed in Figure 3c without further smoothing. The vertical distance is measured in mm, but once again, the origin is placed at an arbitrary location during image calibration. In this figure, the flow reversal in the wake is much more visible and the zero-velocity region is situated approximately 3.5 mm from the fuselage. The locally accelerated flow from the wheel tip is visible just below the origin.

CONCLUSIONS & FUTURE WORK

Boundary layer and wake velocity measurements were performed with 95 μ m resolution around a small aircraft model using LD μ PIV. The vector resolution is sufficient to provide boundary layer profiles, separation bubbles and large-scale flow dynamics, but not yet sufficient to resolve smaller turbulence scales. In order to increase the spatial resolution, a better magnification is required. Similarly, in order to achieve a measurement volume thinner than 380 μ m, PIV lasers with better beam characteristics must be used. For shorter particle response times, the mean particle size should be decreased, and for particle detectability the laser pulse energy density should be increased. Fluorescent imaging can be used to suppress undesired wall reflections, and particle-tracking techniques can enhance resolution and accuracy near the wall. An ensemble average of 61 vector maps is not sufficient to describe turbulence statistics; therefore a larger number of images should be acquired. For increased temporal resolution, high-speed CMOS detectors can be used and high repetition rate Nd:YLF lasers with sufficient pulse energy must be available. These conclusions indicate that LD μ PIV experiments require advanced hardware components for spatially and temporally resolved turbulence measurements. Future experiments will include improved spatial resolution with a larger image ensemble for better turbulence statistics.

ACKNOWLEDGMENTS

The authors extend their thanks to Anadolu Jet Airlines for providing the aircraft model, which is the inspiration for this experiment.

References

- Adrian RJ, Westerweel J (2010) *Particle image velocimetry*, Cambridge University Press, Cambridge
- Dieterle L, Weichert R (1996) *Particle image velocimetry applied to microstructures in turbulent flows*, Engineering Turbulence Modelling & Experiments Vol 3. pp. 391-400
- Fiscaletti D, Elsinga GE, Westerweel J (2013) *Long-range μ PIV in the turbulent region of a jet, at high Reynolds numbers*, Proc. 10th Int. Symp. on Particle Image Velocimetry, Delft, The Netherlands
- Kähler CJ, McKenna R, and Scholz U (2005) *Wall-shear-stress measurements at moderate Re-numbers with single pixel resolution using long distance μ PIV – an accuracy assessment*, 6th International Symposium on Particle Image Velocimetry, Pasadena, CA, Sept. 2005
- Kähler CJ and Scholz U (2006) *Application of long distance MicroPIV at Large Reynolds number*, 13th Int. Symp on Appl. Laser Techniques to Fluid Mechanics, Lisbon, Portugal, Jun 2006
- Kähler CJ, Scholz U and Ortmanns J (2006) *Wall-shear-stress and near-wall turbulence measurements up to single pixel resolution by means of long-distance micro-PIV*, Experiments in Fluids, Vol. 41, pp:327-341
- Lindken R, Di Silvestro F, Westerweel J and Nieuwstadt FTM (2002) *Turbulence measurements with μ -PIV in large scale pipe flow*, Proc. 11th Int. Symp. on Applications of Laser Techniques to Fluid Mechanics, Lisbon, Portugal
- Urushihara T, Meinhart CD, and Adrian RJ (1993) *Investigation of the logarithmic layer in pipe flow using particle image Velocimetry*, Near Wall Turbulence Flows, Elsevier, Amsterdam, The Netherlands, pp:433-446
- Westerweel J and Scarano F (2005) *Universal outlier detection for PIV data*, Exp. In Fluids 39, pp.1096-1100